Applied Magnetic Resonance
https://doi.org/10.1007/s00723-023-01571-6

Applied
Magnetic Resonance

ORIGINAL PAPER

Oil Mobility in Hazelnut Oil-Based Oleogels Investigated by NMR

Lena Trapp[1] · Hilke Schacht[2] · Luisa Eymann[1] · Hermann Nirschl[1] · Gisela Guthausen[1,3]

Received: 25 May 2023 / Revised: 4 July 2023 / Accepted: 14 July 2023

Abstract
The migration of triacyl glycerides such as hazelnut oil leads to quality losses in various foods (e.g., fat bloom formation on chocolate, also named "fat ripening"). Oleogelation, i.e., dispersion of oils in a solid matrix of gelators, is thought to immobilize oils and consequently to hinder oil migration, leading to questions about the translational, but also intramolecular mobility of triacyl glycerides in the oleogels. In addition to translational mobility measured by diffusion-NMR, the molecule-intrinsic dynamics is reflected in NMR-relaxation. In this study, transverse relaxation and diffusion were explored to obtain insight into the condition of the oils in the disperse materials. Oleogels based on sunflower seed wax are compared to oleogels based on mono- and diglycerides. In both types of oleogels NMR-measures depend on composition as well as on temperature. Studying both dimensions, concentration and temperature, reveals the restricted mobility of oil molecules in the oleogels.

1 Introduction

Fats and oils play a fundamental role in texture and structure in many foods [1], and quality losses are known due to migration of triacyl glycerides (TAG), the esters of the trivalent alcohol glycerol (propane-1,2,3-triol) with three fatty acids (FA). Natural fats and oils consist mainly of TAG as well as small amounts of free FA, fat-soluble vitamins and phospholipids, while the chemical structure of FA determines the physico-chemical properties of TAG [2–4]. Migration of TAG is one of

L. Trapp and H. Schacht contributed equally and share the first authorship.

✉ Gisela Guthausen
gisela.guthausen@kit.edu

1 Institute of Mechanical Process Engineering and Mechanics, KIT, 76131 Karlsruhe, Germany

2 Fraunhofer Institute for Process Engineering and Packaging IVV, 85354 Freising, Germany

3 Engler-Bunte-Institut, Water Chemistry and Technology, KIT, 76131 Karlsruhe, Germany

Published online: 18 August 2023

the main reasons of fat bloom, also named fat ripening, in filled chocolates [5]. Nut-based fillings, for example nougat, are especially susceptible [6–8] with hazelnut oil (HNO) as an important component. HNO is rich in unsaturated FA like oleic acid ($C_{18}H_{34}O_2$, C18:1, (9*Z*)-Octadec-9-enoic acid) and linoleic acid ($C_{18}H_{32}O_2$, C18:2, (9*Z*,12*Z*)-Octadeca-9,12-dien acid). HNO has high amounts of liquid TAG, such as 2,3-Bis[{(*Z*)-octadec-9-enoyl}oxy]propyl(*Z*)-octadec-9-enoat, $C_{57}H_{104}O_6$ (OOO), 1,2-Dilinaoyl-3-oleoyl-glycerol (LLO), 1-Linaloyl-2,3-dioleoyl-glycerol (LOO) and 1-Palmitoyl-2,3-dioleoyl-glycerol (POO) [9, 10]. These highly mobile TAG migrate from the chocolate filling into the chocolate shell and dissolve TAG in cocoa butter, which then also migrate to the surface and crystallizes there as fat bloom [5, 8, 11]. NMR methods were applied in different molecular environments as chocolate and oleogels to investigate these phenomena [12–14].

Oleogelation could be a way to reduce oil migration by structuring the edible oils [15]. A three-dimensional network by organogelators (e.g., waxes, mono- and diglycerides or phospholipids) forms, in which the liquid oil is enclosed. Thus, mobile oils are "solidified" without hydrogenation or other chemical modifications [16–19]. The mechanism and extent of gelation depends on the gelator. Organogelators form stable gels even at low concentrations ranging between 1 and 4% ww^{-1} [16]. Wax from sunflower seeds (SFSW) [20, 21] or rice-bran wax [22] form needle-like structures, while mono- and diglyceride (MDG) crystals show rosette-like structures [23]. These structures are characterized on diverse length scales, which becomes also evident in the diffusion experiments of this paper. Typical orders of the gelators clusters include the nanostructure of crystalline nanoplates which assemble into colloidal networks in the range of 1–10 µm up to aggregates in the order of 100 µm [12, 23, 24].

Migration occurs for mobile fats and oils, while immobilized, bounded and partially crystalline fats do not contribute in a first approach, they are thought to hinder other mobile components in migrating [3]. Temperature has a major influence: below the glass transition temperature of the oils and fats, the molecular mobility is small [25, 26]. Above the melting temperature, the thermal energy of the molecules is larger compared to van der Waals forces [26]. Accordingly, the low melting point of most vegetable oils such as sunflower oil or HNO corresponds to high mobility [27].

However, the term 'oil mobility' needs a definition [26]. 'Molecular mobility' is one aspect of the described migration of molecules, often caused by a concentration gradient in a first attempt given by Fick's second law. Brownian motion is due to thermal energy. An important contribution to oil migration is, therefore, translational diffusion. Conventional methods for measuring oil mobility, and synonymously oil binding capacity, like centrifugation or draining on filter paper are not standardized and are performed on soft or molten masses. Extraction and subsequent chromatographic or gravimetric determination of free fat are time consuming. Moreover, these methods do not provide information on the type and extent of oil binding [6, 28]. In the present context, oil binding is understood as change of the oils molecular mobility—either in translational or rotational dynamics—as reflected in diffusion and transverse NMR-relaxation.

NMR-transverse relaxation and diffusion are known for their potential to measure intramolecular mobility as well as translational mobility. Both methods were, therefore, applied to elucidate oil mobility on two different length and time scales and to gain deeper understanding about the immobilization of fats and oils in oleogels. The typical length scale in transverse relaxation concerns the Å to nm region, while the time scale is on the ms range according to the echo time τ_e. In the case of PFG-STE (pulsed field gradient-stimulated echo), the time scale is crudely given by the diffusion time Δ, the length scale corresponds to the root-mean square displacement z of the molecules which in the present case of oils is in the order of several µm on the given time scale. Studies on mobility of free and bound water exist, oils and fats were less investigated in that respect [29, 30]. Temperature-dependent NMR (^{1}H Larmor frequency 400 MHz) was thus used to study HNO in SFSW and MDG oleogels. FA composition, melting- and crystallization behavior, viscosity and the oil binding capacity (OBC) were determined to complete the study and are summarized in the Supplementary Information.

2 Materials and Methods

2.1 Materials

SFSW was obtained from Kahl GmbH & Co. KG (Trittau, Germany). The temperature range for melting is $T_M \in [347, 353]$ K. MDG were extracted from sunflower oil in-house. Virgin HNO was purchased from Reichold Feinkost GmbH (Diez, Germany).

2.2 Sample Preparation

Oleogels were prepared by direct dispersion of the gelator in HNO with concentrations of 5, 7.5 and 10% ww^{-1} SFSW or MDG (shortened to e.g., HNO + 5% SFSW). The mixture was heated to 358 K with a temperature rate of 1.33 $K{\cdot}min^{-1}$ in a temperature-controlled water bath (Julabo GmbH, Seelbach, Germany) while constantly shearing with a speed of 200 min^{-1} by a stirring bar (PHOENIX Instrument, Garbsen, Germany). The dispersion was cooled down to 338 K with a rate of 0.75 $Kmin^{-1}$ using the same equipment. After the mixture reached room temperature without further stirring, it was stored at 277 K for 24 h to allow the oleogel network to form. A detailed characterization is summarized in the Supplementary Information.

2.3 NMR Measurements

2.3.1 Instrumentation and NMR Experiments

NMR experiments were performed on a 400 MHz spectrometer (Avance Neo WB ultrashield, Bruker BioSpin, Germany) with the software Topspin 4.1.1. The

instrument was equipped with a 5-mm DiffBB gradient probe. Samples were tempered by a Variable Temperature Unit (BVT, Bruker BioSpin, Germany). Temperature calibration [31] was performed to correlate the sample temperature T and the BVT temperature. T was measured via the difference in the chemical shift between the –OH and the $–CH_2–$ ^{1}H lines of ethylene glycol (ROTIPURAN®, Carl Roth, Karlsruhe, Germany, purity ≥ 99.5%) [31].

Oleogels and their constituents were measured in 5 mm NMR sample tubes with a filling height of 1 cm to reduce convection especially at elevated temperatures. T was varied in 5 K steps between 298 and 358 K. A holding time of 15 min preceded each NMR measurement. The following sequence of experiments was recorded: ^{1}H-FID (free induction decay) for spectroscopy; PFG-STE NMR for diffusion [32] and CPMG (multi echo sequence according to Carr, Purcell, Meiboom, and Gill [33]) for transverse relaxation. The NMR parameters are listed in Table 1.

In a simple liquid, the PFG-STE magnetization decay of the liquid part follows the Stejskal–Tanner equation [34]:

$$\frac{S}{S_0} = \exp\left(-\gamma^2 g^2 \delta^2 \left(\Delta - \frac{\delta}{3}\right) D\right) = \exp\left(-q^2 \left(\Delta - \frac{\delta}{3}\right) D\right). \quad (1)$$

The signal amplitude S at the gradient amplitude $g = 0$ Tm^{-1} is given by S_0, D is the diffusion coefficient, Δ the diffusion time, and δ the duration of the gradient pulse. q^2 is defined here as an abbreviation of the product $\gamma^2 g^2 \delta^2$, with the gyromagnetic ratio γ. This description allows the identification of diffusion time-dependent effects. Please note that two delays in the stimulated echo sequence require sufficiently long transverse as well as longitudinal relaxation times leading to the fact that only the liquid part of the samples was observed.

Following Bloch equations in the case of "simple" spin systems, the signal decays are described by an exponential decay function characterized by the transverse relaxation rate R_2. Please note that only the liquid part of the dispersed phase was measured in the CPMG experiments due to large R_2 in solids. In the case of ^{1}H NMR on macromolecules, R_2 reflects mainly fluctuating homonuclear

Table 1 Acquisition parameters of the ^{1}H-NMR experiments

	Single Pulse	CPMG	PFG-STE
Number of averages (–)	16	8	8
Number of increments (–)	–	32	32
Acquired data points (–)	16 k	16 k	32 k
Repetition time (s)	5	2.42	2.42
Echo time (s)	–	0.01	–
Diffusion time (s)	–	–	[0.0056, …, 0.4]
Gradient duration (s)	–	–	[0.002, …, 0.0027]
Gradient amplitude (Tm^{-1})	–	–	[0.77, …, 15.49]
Measurement time (min)	1	16.42	[16, …, 17]

dipolar interactions, which are caused by intramolecular mobility, for example, given by the rotational degrees of freedom of $–CH_2–$ groups.

2.3.2 Data Analysis

Oleogels cannot be regarded as "simple" spin systems, which is already evident from their chemical composition and additionally motivated by the state of aggregation of the different components. Thus, signal decays in both, diffusion experiments and relaxation measurements differ from the "simple" modelling sketched above. A variety of modelling approaches of magnetization decays is known like sums of exponential decays, the inverse Laplace transform as well as the discrete distributions of both, R_2 and D. The gamma distribution approach uses discrete, mathematically well described distributions and was applied for multi-component mixtures with molecular weight distributions like oils, gelators and oleogels [35, 36]. A bimodal distribution is needed to describe the PFG-NMR magnetization decays numerically well at temperatures below the melting temperatures $T < T_M$. Transverse magnetization decays were also analyzed via the bimodal gamma distribution model which was established for HNO (Supplementary Information). Reasons for the bimodal distributions are the large variety of molecules with their individual molecular weight distributions and the hinderance and restriction of mobility at the high concentrations in these dispersed systems. All these facts lead to distributions of correlation times and root-mean square displacements of ^1H spin bearing functional groups. The signal decays of PFG-STE and CPMG experiments were modeled within Origin 2021 (OriginLab Corporation, Northampton, United States) using the Levenberg–Marquardt iteration algorithm. The coefficient of determination R^2 was larger than 99%.

At melting and crystallization temperatures T_M and T_C, the microstructure in the oleogels changes. Below T_M and T_C, diffusion described by $D_{eff}(\Delta)$ depends on the diffusion time Δ due to geometric hindrance and interactions of the oil molecules with the gelators. The tortuosity model [37–39] was applied similar to the findings in hydrogels [40] and in lubricating greases [41, 42]. The current conception is that the effective guest molecule diffusion depends on Δ due to the gelator networks resulting in an effective tortuosity $\tau_{tort} > 1$. A second parameter in the model is the surface-to-volume ratio SV^{-1} [37]. SV^{-1} refers to the structure of the gelator. The model's parameter could be explored to improve the stability, texture and shelf life of gelator-containing products. A quantitative impression is given by additionally calculate the effective root-mean square displacement z of the oil molecules, which depends on Δ and $D_{eff}(\Delta)$:

$$z = \sqrt{2 \cdot D_{eff}(\Delta) \cdot \Delta}. \tag{2}$$

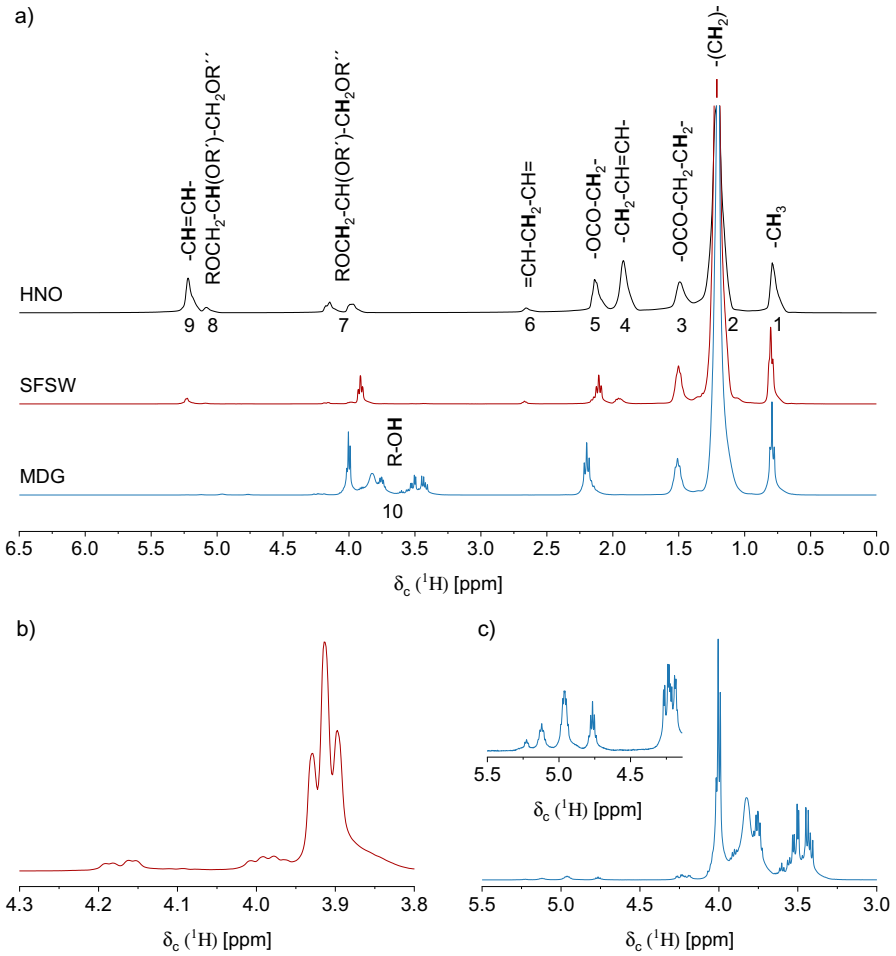

Fig. 1 **a** ^{1}H-NMR spectra of HNO (black), SFSW (red) and MDG (blue) at $T > 353$ K. All spectra are dominated by peak 2 attributed to $–CH_2–$ groups. The zooms show the characteristic ^{1}H lines of the gelators **b** SFSW and **c** MDG. ^{1}H signals at 3.3–5.3 ppm are attributed to glyceryl and other alcohols

3 Results and Discussion

Attempts to diminish fat bloom and quality losses in chocolate explore geometric restriction and hinderance of especially HNO in dispersed systems such as oleogels [43]. By combining NMR relaxation and diffusion, complementary information is obtained about binding and mobility of HNO in the oleogels: While R_2 is determined by low frequency fluctuations of mainly the dipolar interactions within a molecule, diffusion provides insight into the translational mobility.

3.1 ^{1}H-NMR Spectra of the Constituents of the Oleogels: HNO and Gelators

The temperature-dependent structuring and influence of the gelator was detected via ^{1}H-NMR spectroscopy (Fig. 1). Melting, solidification, and structural stability of compositions can be quantitatively observed. ^{1}H spectra of HNO (Fig. 1a) at room temperature were assigned in accordance with [44–46] (Table 2). Oleic acid was identified as main component by gas chromatography (GC) (Table SI 1, Supplementary Information) as well as by ^{1}H-NMR: ^{1}H bound to allylic carbons (peak 4) and the olefinic ^{1}H (peak 9). The two gelators SFSW and MDG are organic solids where mainly dipolar interactions lead to line broadening. $T > 353$ K, above T_M, was used for the spectra in Fig. 1. Unique, characteristic ^{1}H lines are in the chemical shift range of 3.8–4.0 ppm for SFSW (Fig. 1b) and in the range of 3.0–5.5 ppm for MDG (Fig. 1c). Lines at 3.3–5.3 ppm were attributed to glyceryl [47] and other alcohols. All ^{1}H spectra are dominated by the signature of $–CH_2–$ groups with the highest signal intensity of about 60% (Fig. 1, peak 2). Transverse relaxation and diffusion were measured for this dominant line to study oil mobility in oleogels.

3.2 Oleogels

Oil mobility is expected to be sensitive to temperature, but also to the type of gelator. The gelators in the oleogels will not significantly contribute to the measured liquids signal decays due to the small S_0 or fast transverse relaxation at low temperatures (Supplementary Information). The concentration compared to HNO is also small. MDG oleogels are thereby expected to melt at lower T than SFSW oleogels (Differential scanning calorimeter (DSC), Fig. SI 2, Supplementary Information).

3.2.1 Transverse Relaxation in Oleogels

HNO is expected to interact with the gelator in oleogels with consequences for R_2. For example, R_2 of the liquid oil phase in a fat matrix was shown to be influenced by surface relaxation caused by crystal surfaces [48]. The gelators phase transition should thus be observable in R_2.

The transverse signal decays of $–CH_2–$ groups in the oleogels (Fig. 2) significantly differ from those of HNO (Fig. SI 4 and SI 5, Supplementary Information). They were modelled with the bimodal gamma distribution model (Figs. 2, 3). The mean relaxation rates of both types of oleogels are larger than those of HNO at $T < T_M$ [oleogels: $<R_{2,1}> \in$ [10, 14] s^{-1} and $<R_{2,2}> \in$ [4, 7] s^{-1}, compared to HNO: $<R_{2,1}> \in$ [7, 11] s^{-1} and $<R_{2,2}> \in$ [2, 4] s^{-1} (Supplementary Information)]. As expected, the intramolecular mobility is reduced in all oleogels compared to HNO when the gelator is in its solid form. The solid–liquid phase transition shifts to lower T with increasing gelator concentration. In addition, the phase transition occurs at lower T for MDG compared to SFSW oleogels in agreement with the expectations (DSC, Fig. SI 2, Supplementary Information).

At $T < T_M$, differences between the two types of oleogels are obvious: While $<R_{2,i}>$ of MDG oleogels monotonically decrease with increasing T (T

Table 2 ^{1}H chemical shift assignments of the main components in the oleogels: HNO, SFSW and MDG

Peak	1	2	3	4	5	6	7	8	9	10
δ_c (ppm)	0.8–0.9	1.2–1.4	1.6–1.7	2.0–2.1	2.2–2.4	2.7–2.8	4.1–4.3	5.2	5.3–5.4	3.3–5.3
Compound	Terminal methyl group	Methylene	Methylene group in ß-position of carbonyl group	Allylic carbons	Methylene group in α-position of carbonyl group	Bis-allylic carbons	Glycerol group in sn-1,3 position	Glycerol group in sn-2 position	Olefinic	Other alcohols
^{1}H in the functional group	–C**H**$_3$	–(C**H**$_2$)–	–OCO–CH$_2$– C**H**$_2$–	–C**H**$_2$– CH=CH–	–OCO–C**H**$_2$–	=CH–C**H**$_2$– CH=	ROC**H**$_2$– CH(OR′)– C**H**$_2$OR″	ROCH$_2$– C**H**(OR′)– CH$_2$OR′	–C**H**=C**H**–	R-O**H**
HNO	X	**X**	X	X	X	X	X	X	x	
SFSW	X	**X**	X	x	X	x	x	x	x	x
MDG	X	**X**	X		X		**X**	x		x

"x" marks the presence of the functional group in the spectrum of the respective species. A distinction is made between bold (**X**), large (X) and small (x) representing the proportion of the functional group in the spectra

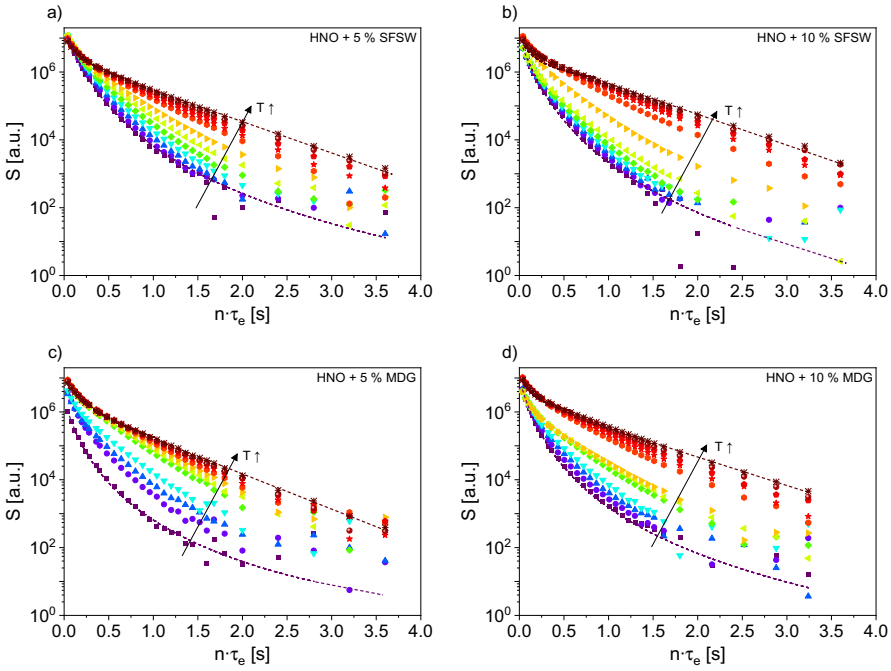

Fig. 2 Logarithmic $-CH_2-$ CPMG magnetization decays ($\tau_e = 0.01$ s) of HNO in **a** 5% SFSW, **b** 10% SFSW, **c** 5% MDG and **d** 10% MDG for $T \in [298, 353]$ K: 298 K (◊), 303 K (◦), 308 K (▽), 313 K (▷), 318 K (△), 323 K (○), 328 K (▷), 333 K (□), 338 K (◇), 343 K (□), 348 K (□), 353 K (□) with fits according to the bimodal gamma distribution for the extremes in temperatures

$\in [298, 333]$ K, $T < T_M$), $< R_{2,i} >$ of HNO + 10% SFSW are approximately constant up to $T = 328$ K ($T < T_M$). $< R_{2,1} > \in [11–14]$ s^{-1} for the MDG oleogel are larger than that for the SFSW oleogel with $< R_{2,1} > \in [10, 12]$ s^{-1} at $T \in [298, 308]$ K, which suggests a stronger interaction in the nearest neighbourhood of gelator and oil molecules. MDG oleogels are thus more temperature sensitive than SFSW oleogels. At $T > T_M$, relaxation rates are comparable to those of HNO (oleogels: $< R_{2,1} > \in [7, 9]$ s^{-1} and $< R_{2,2} > \in [2, 4]$ s^{-1}) due to the melting of the gelators and consequently the disassembling of the gel network.

3.2.2 Diffusion in Oleogels

The solid phase of the gelators is considered to geometrically hinder HNO diffusion as it was early described in [49]. Oil diffusion in fat crystal matrices was found to be influenced by the pore space in a fat network [48]. Other parameters are the tortuosity τ_{tort} of the network, the capillary flow, the diffusion of the liquid oil, the oil viscosity and the contact area between liquid and solid [48]. Different length scales must be considered: Clusters and particles on the length scale of several 10 µm form aggregates in the order of 100 µm [24] apart from the mentioned nanostructures. The aggregates concentration and their distribution as well as the pore size distribution determine the effective oil diffusion. PFG-NMR was thus measured on oleogels

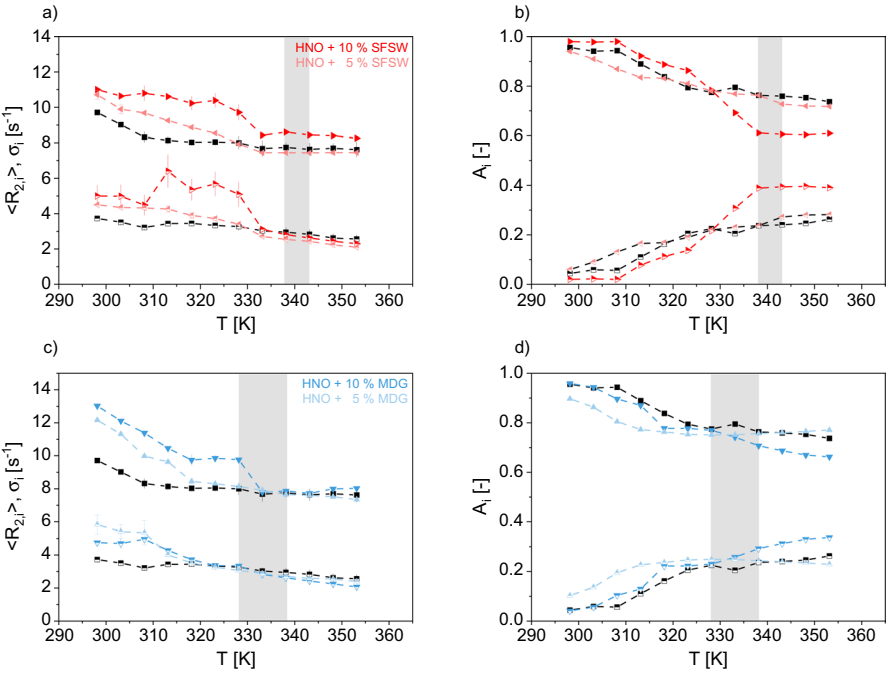

Fig. 3 **a**+**c** $<R_{2,1}> \in$ [7, 14] s^{-1} (filled symbols) and $<R_{2,2}> \in$ [2, 7] s^{-1} (half-filled symbols) with σ_1 and σ_2 (vertical lines), **b**+**d** A_1 (filled symbols) in the range [60, 98] % and $A_2 = 1 - A_1$ (half-filled symbols) of the oleogels HNO + 5% SFSW (top, View), HNO + 10% SFSW (to, Ω), HNO + 10% SFSW (top, β) and HNO + 5% MDG (bottom, ⁊), HNO + 10% MDG (bottom, Β), all values are shown in comparison to HNO (as a function of $T \in$ [298, 353] K. $<R_{2,i}>$ of both oleogels are larger than those of HNO at $T < T_M$. The grey areas indicate the solid–liquid phase transition of pure gelators as revealed by $<R_2>$

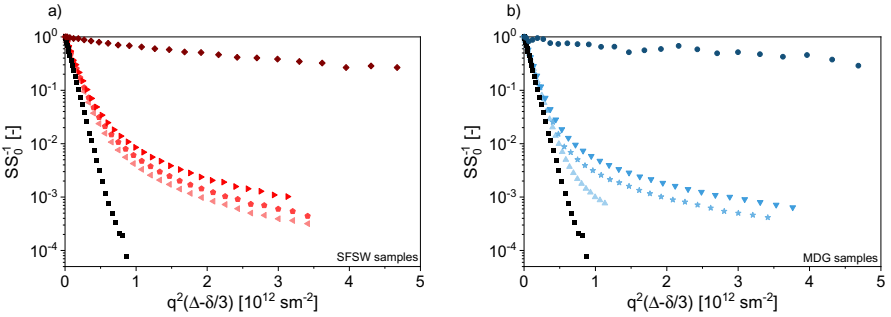

Fig. 4 Normalised –CH_2– magnetization decays in diffusion experiments (Eq. 1, Δ = 120 ms) of HNO-based oleogels with **a** SFSW (5% (Ω), 7.5% (ב), 10% (β)) and **b** MDG (5% (⁊), 7.5% (ξ), 10% (Β)) in comparison to HNO (!), SFSW (Λ) and MDG (›) at $T = 298$ K. The mainly HNO signal in the oleogels depends on type and concentration of the gelator and shows the signature of geometric hindrance

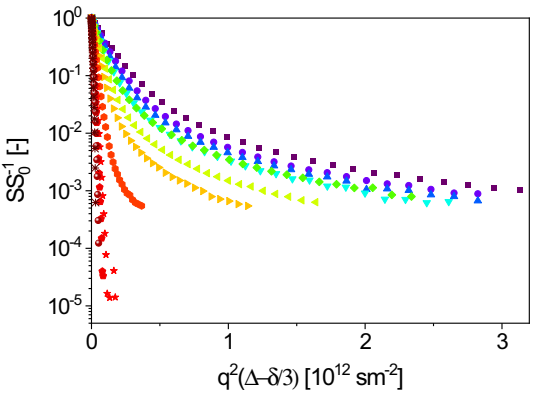

Fig. 5 Normalised $-CH_2-$ PFG-STE magnetization decays of HNO + 10% SFSW, the shape of the normalised signal decays varies as a function of $T \in [298, 353]$ K: 298 K (ι), 303 K (ϸ), 308 K (7), 313 K (B), 318 K (Λ), 323 K (Ω), 328 K (β), 333 K (μ), 338 K (ξ), 343 K (□), 348 K (□), 353 K (□)

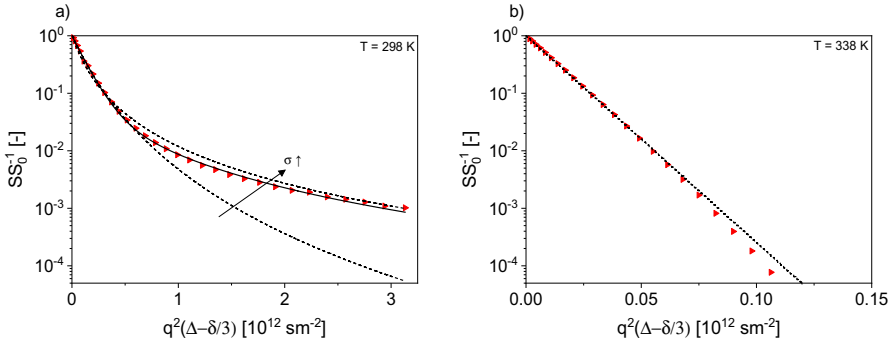

Fig. 6 Exemplarily for PFG-signal decays in oleogels together with the modelled distributions: Normalised $-CH_2-$ magnetization decays of HNO + 10% SFSW (β) at **a** $T = 298$ K ($T < T_M$): The monomodal gamma distribution describes the data not sufficiently well, decays were calculated with different distribution widths (dotted lines), the data are better described by a bimodal gamma distribution (solid line). **b** $T = 338$ K ($T > T_M$): The monomodal gamma distribution (dotted line) describes the data well with an error in the order of 10^{-3}

with 5%, 7.5% and 10% ww^{-1} SFSW (Fig. 4a) and MDG (Fig. 4b) at $T = 298$ K and $\Delta = 120$ ms.

The PFG-signal decay of HNO in the oleogels is less pronounced than that of pure HNO (Fig. 4). Molecular diffusion seems to be hindered and is sensitive to the gelator's type and concentration: HNO diffusion in MDG oleogels is faster than that in SFSW oleogels. When choosing a suitable model for quantification, it should be considered that the shape of the oleogels' signal decay significantly changes. This is obvious in its T-dependence due to the gelators' solid–liquid phase transition (Fig. 5).

Diffusion data are described by bimodal distributions at $T < T_M$. The form of the signal decay is caused by hindered diffusion and molecular diversity. Interactions on the molecular length scale cannot be excluded which lead to diminished diffusion. The simple sum of diffusion distributions of HNO and gelators as well as a monomodal distribution are numerically not sufficient. Two independent contributions

need to be assumed (Fig. 6a). Only at $T > T_M$, modelling by a monomodal gamma distribution (Fig. 6b) is sufficient.

$< D_{eff,1} >$ is smaller than $< D_{eff} >$ of pure HNO in all oleogels. HNO diffusion is more reduced in SFSW ($< D_{eff,1} > \in [8.96 \cdot 10^{-12}, 9.51 \cdot 10^{-12}]$ $m^2 s^{-1}$ and $A_1 \approx 0.90$) than in MDG oleogels at the same gelator concentration ($< D_{eff,1} > \in [9.79 \cdot 10^{-12}, 1.06 \cdot 10^{-11}]$ $m^2 s^{-1}$ and $A_1 \approx 0.96$). Moreover, $< D_{eff,1} >$ decreases with gelator concentration as expected. Concerning the second component in the oleogels: $< D_{eff,2} > \in [3.17 \cdot 10^{-12}, 4.95 \cdot 10^{-12}]$ $m^2 s^{-1}$ is larger than $< D_{eff} >$ of the gelators. $< D_{eff,2} >$ may be attributed to HNO in direct interaction to gelator structures. This fraction of the total magnetisation decay is small with $A_2 \approx 0.1$ for SFSW oleogels and $A_2 \approx 0.04$ for MDG oleogels.

To estimate the HNO hindrance within the three-dimensional gelator networks the root-mean square displacement $z(\Delta = 120$ ms) (Eq. 2) was calculated at $T = 298$ K, (Table 3): $< D_{eff} > = 1.20 \cdot 10^{-11}$ $m^2 s^{-1}$ results in $z = 1.69$ µm for pure HNO. Comparing z of pure HNO with the faster diffusing, larger fraction of HNO in oleogels, $z(< D_{eff,1} >)$ of the oil molecules in oleogels is slightly reduced (Table 3, $z < 1.60$ µm).

The extend of geometric hindrance of diffusion depends on the physical dimensions in the gelators' network. Scanning electron microscope (SEM) images and polarisation microscope images [23, 43, 50] indicate the diverse typical length scales of the solid oleogels which are distributed over a wide range, but significant structures also are in the range of 50 µm for MDG and SFSW, a significantly larger dimension than the calculated z. However, the multiscalar structure of oleogelators needs to be considered making a direct interpretation of z in terms of interaction probability and geometric hindrance length difficult.

Temperature T is an important factor for HNO diffusion in oleogels which is exemplified on the oleogel HNO + 10% ww^{-1} SFSW (Fig. 7): $< D_{eff,1} >$ in the oleogel is smaller than that for pure HNO at $T < T_M$. $< D_{eff,2} > (A_2 \approx 0.1)$ in the oleogel is comparable to $< D_{eff} >$ of the gelator SFSW for $T \in [298, 333]$ K. At $T > T_M$, $< D_{eff} >$ of all substances show similar values when modelled with a

Table 3 Mean effective diffusion coefficients, distribution widths, amplitudes and root-mean square displacement of HNO, SFSW, MDG and oleogels at $T = 298$ K

	$< D_{eff,1} >$ [$m^2 s^{-1}$]	σ_1 ($m^2 s^{-1}$)	A_1 (–)	z_1 (µm)	$< D_{eff,2} >$ ($m^2 s^{-1}$)	σ_2 [$m^2 s^{-1}$]	A_2 (–)	z_2 (µm)
HNO	1.20×10^{-11}	8.09×10^{-18}	1	1.69	–	–	–	–
SFSW	4.95×10^{-13}	4.31×10^{-13}	1	0.35	–	–	–	–
MDG	5.77×10^{-13}	8.01×10^{-13}	1	0.37	–	–	–	–
HNO +								
5% SFSW	9.51×10^{-12}	3.94×10^{-16}	0.93	1.51	4.95×10^{-12}	3.23×10^{-12}	0.07	1.09
7.5% SFSW	9.16×10^{-12}	4.52×10^{-17}	0.89	1.48	4.81×10^{-12}	2.70×10^{-12}	0.11	1.07
10% SFSW	8.96×10^{-12}	3.36×10^{-16}	0.86	1.47	4.46×10^{-12}	2.83×10^{-12}	0.13	1.04
5% MDG	1.06×10^{-11}	5.54×10^{-15}	0.97	1.59	3.17×10^{-12}	6.39×10^{-18}	0.03	0.87
7.5% MDG	1.03×10^{-11}	3.12×10^{-15}	0.97	1.57	4.78×10^{-12}	3.88×10^{-12}	0.03	1.07
10% MDG	9.79×10^{-12}	5.50×10^{-18}	0.94	1.53	4.87×10^{-12}	3.54×10^{-12}	0.06	1.08

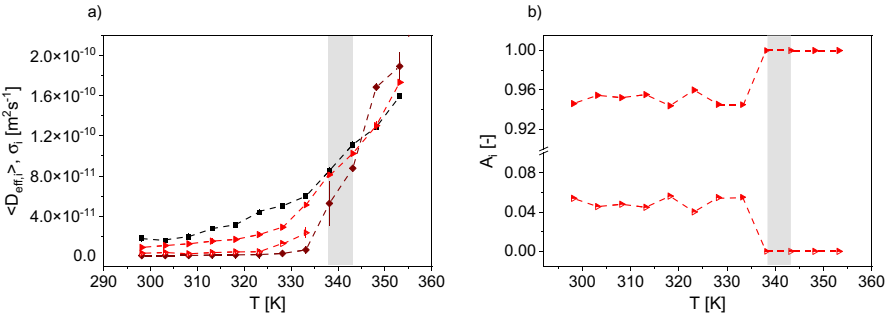

Fig. 7 **a** $<D_{eff,i}>$ and σ_i (vertical lines) of HNO (!), SFSW (Λ) and the oleogel HNO + 10% SFSW (β). $<D_{eff,1}>$ in the oleogel is smaller, $<D_{eff,2}>$ is comparable to $<D_{eff}>$ of SFSW at $T < T_M$. **b** A_i are T-independent below T_M for HNO + 10% SFSW. $A_2(<D_{eff,2}>) \approx 0.1$ is significantly smaller than $A_1(<D_{eff,1}>)$

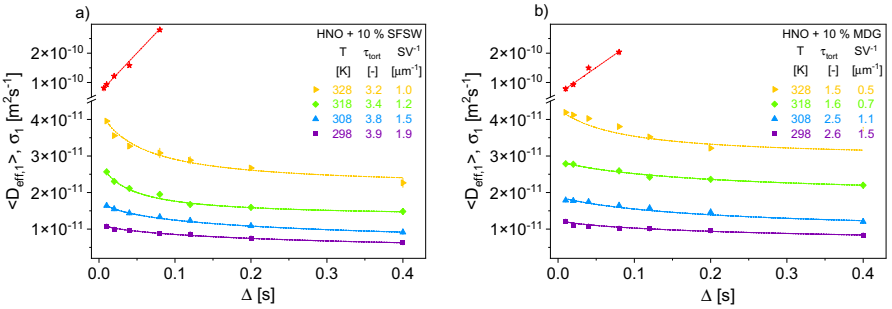

Fig. 8 $<D_{eff,1}>$ and σ_1 (vertical lines) of the –CH_2– peak of **a** HNO + 10% SFSW and **b** HNO + 10% MDG as a function of Δ. $T < T_M$: The data were modelled by the tortuosity model (dotted lines), revealing $\tau_{tort}(T)$ and $SV^{-1}(T)$ in a first attempt. Above T_M (red points, line: guide to the eye), $<D_{eff,1}>$ increases with Δ due to convection

monomodal gamma distribution. Summarizing, diffusion of HNO is reduced by the gelator, but not completely restricted as in droplets of emulsions [51, 52].

$<D_{eff,1}>$ in oleogels depends not only on T, but also on Δ (Fig. 8). The gelator represents a geometric hindrance for HNO molecules, so that diffusion is not free, but hindered. Motivated by the structural similarity to structures such as to hydrogels [40] and lubricant greases [41], the diffusion of oil molecules is interpreted as a function of Δ via the tortuosity model [37] (Fig. 8). Often, the length scales of the root-mean square displacement of the molecules are in the order of the restricting geometry (in [37] $dz^{-1} < 5$, while d is the sphere's diameter). The restricting geometry in the oleogels is, however, multi-facetted: Taking a closer look to the images, for example in [23], structures on the small length scales of 1–5 µm are visible apart from the aggregates dimensions in the order of 50 µm and more. While knowing about the fact that the diffusing moieties should emphasis the restricting geometry, the experimental findings in the images and of the diffusion experiments

show the applicability of the tortuosity model at least as a first attempt to describe the data and being able to compare the measured data on the different oleogels reliably. The tortuosity model [37, 38] results in $\tau_{tort} = 3.9$ and in a surface-to-volume ratio $SV^{-1} = 1.9\ \mu m^{-1}$, exemplarily for the oleogel with 10% SFSW, and $\tau_{tort} = 2.6$, $SV^{-1} = 1.5\ \mu m^{-1}$ for the MDG oleogel (10%) at $T = 298$ K. For further interpretation, we assume a geometric diffusion hinderance of the oil molecules by spherical particles. A value $SV^{-1} = 2\ \mu m^{-1}$ would then correspond to a diameter of a sphere of 1.5 µm. Please note the different length scales in the solid state of oleogels [43] which comprise also the scale of a few µm, while the large structures of mainly agglomerates are in the order of 50 µm. The geometric hindrance reflected in τ_{tort} is larger in SFSW oleogels than in MDG oleogels while SV^{-1} is in the same order of magnitude. Compared to greases and polysaccharide hydrogels, τ_{tort} in oleogels is significantly larger [40–42] and in a similar order of magnitude than observed in porous rocks ($\tau_{tort} \in [3.2, 4.4]$) [39].

The parameters τ_{tort} and SV^{-1} change significantly with T and depend on the oleogels composition. SV^{-1} usually depends on the microscopic structures and sizes. In general, the higher the density the lower SV^{-1}. SV^{-1} is an important parameter and enters the thermodynamic and kinetic descriptions, including that of melting and boiling points, solubility and reactivity and in consequence the applicability range of a dispersed system.

The described findings in oleogels are similar to those of fats [24, 48, 53]. The fat becomes more fluid, occupies more space when melting, and SV^{-1} decreases. TAG-based fat crystals tend to have a dense spherical structure and a relatively small SV^{-1} on the order of 0.3–0.4 μm^{-1}. In contrast, crystalline structures of phospholipids show a larger SV^{-1}, typically in the range 0.5–2 μm^{-1} [24, 54, 55]. Values are also available for waxes: Canauba wax has a typical crystal structure in the form of spherical aggregates with $SV^{-1} \in [0.1, 0.2]\ \mu m^{-1}$. On the other hand, beeswax has a hexagonal crystal structure with $SV^{-1} \in [0.5, 1.0]\ \mu m^{-1}$ [56–58]. Since SFSW can adopt different crystal structures like prismatic and needle-like crystals, $SV^{-1} \in [0.5, 1.5]\ \mu m^{-1}$ was found for prismatic crystals and $SV^{-1} \in [1.0, 2.5]\ \mu m^{-1}$ for needle-like crystals [24, 59–61]. The data could be interpreted in the following way: SFSW appears in a needle-like structure at $T < T_M$, and the structure changes to prismatic crystals just before melting occurs. MDG also form a variety of crystal structures [62]. 1-hexadecanoyl-sn-glycerol can form needles, plates, or crystal aggregates with typical values of $SV^{-1} \in [1.0, 2.0]\ \mu m^{-1}$. Di(octadecanoyl) hexadecan forms needles or hexagonal plates with $SV^{-1} \in [0.5, 1.0]\ \mu m^{-1}$. 1,3-di(octadecanoyloxy)propan-2-yl octadecanoate forms hexagonal plate shapes or prismatic crystals with $SV^{-1} \in [0.3, 0.5]\ \mu m^{-1}$ [24, 59–61]. MDG oleogels seem to have needle-like or plate-like structures for $T < T_M$. For $T > T_M$, convection shows up indicated by $< D_{eff,1} >$ increasing with Δ. This well-known artefact of convection in diffusion data is caused by temperature gradients within the liquid sample, for example [63]. The observation thus is a clear indicator for the solid–liquid phase transition with its impact on oil migration and mobility.

4 Conclusions

Oleogels are disperse systems with hazelnut oil (HNO) as quasi-continuous and the gelators as dispersed phase. NMR was applied to measure oil mobility in oleogels composed of HNO and the gelators mono-diglyceride (MDG) and sunflower seed wax (SFSW). ^{1}H-spectroscopy served as a basis for transverse relaxation measured by CPMG and diffusion measured by PFG-STE. Based on the –CH_2– peak with up to 60% of the ^{1}H signal, a quantitative analysis was made. Diffusion of HNO molecules is more restricted in SFSW oleogels compared to MDG oleogels and is slower at higher gelator concentrations. PFG-STE allowed to quantitatively deduce the tortuosity in the range of $\tau_{tort} \in [1.5, 3.9]$. The solid–liquid phase transitions were observed and are in agreement with findings in differential scanning calorimetry. At temperature below the melting temperatures $T < T_M$, the tortuosity model was applied and reveals τ_{tort} with values larger than in hydrogels and lubricant greases, but similar to values observed in classic porous systems. The findings are in accordance to scanning electron microscope images and polarisation microscopy. HNO diffusion in oleogels is thus hindered but not completely restricted as in droplets of emulsions. Fat ripening will, therefore, be hampered but not excluded. Above the melting temperature of the gelators ($T > T_M$), diffusion resembles that of oil mixtures characterized by an average diffusion coefficient with the expected sensitivity to convection.

Composition and temperature influence also transverse relaxation of HNO in oleogels. All decays were modelled by bimodal gamma distributions. At $T < T_M$, the –CH_2– magnetization decays are dominated by HNO, while both, gelator and HNO determine the decays at $T > T_M$. The solid–liquid phase transition becomes obvious on the time and length scales of transverse NMR relaxation. The phase transition in oleogels shifts to higher temperatures with gelator concentration in agreement with differential scanning calorimetry.

Supplementary Information The online version contains supplementary material available at https://doi.org/10.1007/s00723-023-01571-6.

Acknowledgement The authors thank the German Federation of Industrial Research Association (AiF) for financial support of the research project IGF-Nr. 21785 N. This project was carried out under the auspices of AiF and financed within the budget of the Federal Ministry of Economic Affairs and Climate Action (BMWK) through the program to promote collective industrial research (IGF). The Deutsche Forschungsgemeinschaft is acknowledged for the substantial financial contribution in form of NMR instrumentation and within the instrumental facility Pro2NMR. Kahl GmbH & Co. KG (Trittau, Germany) kindly provided SFSW. The publication is a dedication to Bernhard Blümich - on the occasion of his 70th birthday.

Author Contributions Conceptualization and methodology LT, HS, and GG; data curation, investigation LT, HS, LE; resources, HN, GG; visualization and writing—original draft preparation, LT, HS, GG; writing—review and editing, LT, HS, LE, HN, GG; supervision, funding acquisition HN, GG; all authors have read and agreed to the published version of the manuscript.

Funding Open Access funding enabled and organized by Projekt DEAL. This research was funded by the German Federal Ministry of Economic Affairs and Climate Action (BMWK) through the program to promote collective industrial research (IGF) with the German Federation of Industrial Research Association (AiF), IGF-Nr. 21785 N. The responsibility for the content of this publication lies with the author.

Availability of Data and Materials The data are available on request to the authors.

Declarations

Conflict of interest The authors have declared no conflict of interest.

Ethical approval Not applicable.

References

1. G.G. Rye, J.W. Litwinenko, A.G. Marangoni, Fat crystal networks, in *Bailey's Industrial Oil and Fat Products*, ed. by F. Shahidi (Wiley-Interscience, Hoboken, 2005)
2. M. Bockish, Composition, structure, physical data, and chemical reactions of fats and oils, their derivatives, and their associates, in *Fats and Oils Handbook* (1998), pp. 53–120
3. R. Miklos, H. Mora-Gallego, F.H. Larsen, X. Serra, L.Z. Cheong, X. Xu, J. Arnau, R. Lametsch, Influence of lipid type on water and fat mobility in fermented sausages studied by low-field NMR. Meat Sci. **96**, 617–622 (2014)
4. M.A. Rogers, A.J. Wright, A.G. Marangoni, Engineering the oil binding capacity and crystallinity of self-assembled fibrillar networks of 12-hydroxystearic acid in edible oils. Soft Matter **4**, 1483–1490 (2008)
5. G. Ziegleder, C. Moser, J. Geier-Greguska, Kinetics of fat migration within chocolate products. Part I: Principles and analytics. Fett-Lipid **98**, 196–199 (1996)
6. G.R. Ziegler, A. Shetty, R. Anantheswaran, Nut oil migration through chocolate. Manuf. Confect. **84**, 118–126 (2004)
7. S. Cikrikci, M.H. Oztop, Oil migration in hazelnut paste/chocolate systems using magnetic resonance imaging. J. Food Meas. Charact. **12**, 1460–1472 (2018)
8. R.S. Khan, D. Rousseau, Hazelnut oil migration in dark chocolate–kinetic, thermodynamic and structural considerations. Eur. J. Lipid Sci. Technol. **108**, 434–443 (2006)
9. J. Sun, X. Feng, C. Lyu, S. Zhou, Z. Liu, Effects of different processing methods on the lipid composition of hazelnut oil: a lipidomics analysis. Food Sci. Hum. Wellness **11**, 427–435 (2022)
10. C. Alasalvar, J.S. Amaral, F. Shahidi, Functional lipid characteristics of Turkish Tombul hazelnut (*Corylus avellana* L.). J. Agric. Food Chem. **54**, 10177–10183 (2006)
11. M.E. Miquel, S. Carli, P.J. Couzens, H.-J. Wille, L.D. Hall, Kinetics of the migration of lipids in composite chocolate measured by magnetic resonance imaging. Food Res. Int. **34**, 773–781 (2001)
12. N.C. Acevedo, B. MacMillan, B. Newling, A.G. Marangoni, Shear effects on the diffusive movement of oil in triacylglycerol networks. RSC Adv. **7**, 1634–1642 (2017)
13. K. Deka, B. MacMillan, G.R. Ziegler, A.G. Marangoni, B. Newling, B.J. Balcom, Spatial mapping of solid and liquid lipid in confectionery products using a 1D centric SPRITE MRI technique. Food Res. Int. **39**, 365–371 (2006)
14. A.G. Marangoni, B. MacMillan, S. Marty, B.J. Balcom, Spatial mapping of solid and liquid lipid in chocolate, in *Magnetic Resonance in Food Science*, eds. by M. Gudjonsdottir, P. Belton, G. Webb (RSC Publishing, Cambridge, 2009)
15. A.G. Marangoni, Organogels: an alternative edible oil-structuring method. J. Am. Oil. Chem. Soc. **89**, 749–780 (2012)

16. A.I. Blake, E.D. Co, A.G. Marangoni, Structure and physical properties of plant wax crystal networks and their relationship to oil binding capacity. J. Am. Oil. Chem. Soc. **91**, 885–903 (2014)
17. J. Li, H. Yu, Y. Yang, C.J. Drummond, C.E. Conn, Effect of crystallization state on the gel properties of oleogels based on β-sitosterol. Food Biophys. **16**, 48–57 (2021)
18. Y. Shi, C. Liu, Z. Zheng, X. Chai, W. Han, Y. Liu, Gelation behavior and crystal network of natural waxes and corresponding binary blends in high-oleic sunflower oil. J. Food Sci. **86**, 3987–4000 (2021)
19. A.R. Patel, K. Dewettinck, Edible oil structuring: an overview and recent updates. Food Funct. **7**, 20–29 (2016)
20. M. Öğütcü, E. Yılmaz, Characterization of hazelnut oil oleogels prepared with sunflower and carnauba waxes. Int. J. Food Prop. **18**, 1741–1755 (2015)
21. H.S. Hwang, S. Kim, M. Singh, J.K. Winkler-Moser, S.X. Liu, Organogel formation of soybean oil with waxes. J. Am. Oil. Chem. Soc. **89**, 639–647 (2012)
22. L.S.K. Dassanayake, D.R. Kodali, S. Ueno, K. Sato, Physical properties of rice bran wax in bulk and organogels. J. Am. Oil. Chem. Soc. **86**, 1163–1173 (2009)
23. E. Kesselman, E. Shimoni, Imaging of oil/monoglyceride networks by polarizing near-field scanning optical microscopy. Food Biophys. **2**, 117–123 (2007)
24. A. Patel, *Alternative Routes to Oil Structuring* (2015).
25. T. Labuza, C. Hyman, Moisture migration and control in multi-domain foods. Trends Food Sci. Technol. **9**, 47–55 (1998)
26. G. Roudaut, D. Simatos, D. Champion, E. Contreras-Lopez, M. Le Meste, Molecular mobility around the glass transition temperature: a mini review. Innov. Food Sci. Emerg. **5**, 127–134 (2004)
27. R. Miklos, L.-Z. Cheong, X. Xu, R. Lametsch, F.H. Larsen, Water and fat mobility in myofibrillar protein gels explored by low-field NMR. Food Biophys. **10**, 316–323 (2015)
28. H. Bertram, H. Andersen, A. Karlsson, Comperative study of LF-NMR relaxation measurements and two traditional methods in the determination of water holding capacity of pork. Meat Sci. **57**, 125–132 (2001)
29. J.P. Peters, F.J. Vergeldt, H. Van As, H. Luyten, R.M. Boom, A.J. Van der Goot, Time domain nuclear magnetic resonance as a method to determine and characterize the water-binding capacity of whey protein microparticles. Food Hydrocolloids **54**, 170–178 (2015)
30. H. Todt, G. Guthausen, W. Burk, D. Schmalbein, A. Kamlowski, Water/moisture and fat analysis by time-domain NMR. Food Chem. **96**, 436–440 (2006)
31. R.E. Hoffman, E.D. Becker, Temperature dependence of the 1H chemical shift of tetramethylsilane in chloroform, methanol, and dimethylsulfoxide. J. Magn. Reson. **176**, 87–98 (2005)
32. J.E. Tanner, Use of stimulated echo in NMR-diffusion studies. J. Chem. Phys. **52**, 2523–3000 (1970)
33. S. Meiboom, D. Gill, Modified spin-echo method for measuring nuclear relaxation times. Rev. Sci. Instrum. **29**, 688–691 (1958)
34. E.O. Stejskal, J.E. Tanner, Spin diffusion measurements: spin echoes in the presence of a time-dependent field gradient. J. Chem. Phys. **42**, 288–292 (1965)
35. M. Röding, D. Bernin, J. Jonasson, A. Sarkka, D. Topgaard, M. Rudemo, M. Nyden, The gamma distribution model for pulsed-field gradient NMR studies of molecular-weight distributions of polymers. J. Magn. Reson. **222**, 105–111 (2012)
36. M. Röding, N. Williamson, M. Nydén, Gamma convolution models for self-diffusion coefficient distributions in PGSE NMR. J. Magn. Reson. **261**, 6–10 (2015)
37. L.L. Latour, P.P. Mitra, R.L. Kleinberg, C.H. Sotak, Time-dependent diffusion-coefficient of fluids in porous-media as a probe of surface-to-volume ratio. J. Magn. Reson. A **101**, 342–346 (1993)
38. P.P. Mitra, L.L. Latour, R.L. Kleinberg, C.H. Sotak, Pulsed-field-gradient NMR measurements of restricted diffusion and the return-to-the-origin probability. J. Magn. Reson. A **114**, 47–58 (1995)
39. L. Latour, R.L. Kleinberg, P.P. Mitra, C.H. Sotak, Pore-size distributions and tortuosity in heterogeneous porous media. J. Magn. Reson. A **112**, 83–91 (1995)
40. F. Junker, K. Michalski, G. Guthausen, M. Bunzel, Characterization of covalent, feruloylated polysaccharide gels by pulsed field gradient-stimulated echo (PFG-STE)-NMR. Carbohydr. Polym. **267**, 118232 (2021)
41. T. Rudszuck, N. Schork, H. Nirschl, G. Guthausen, Nuclear magnetic resonance/magnetic resonance imaging on lubricating greases: observation of bleeding and aging. Magn. Reson. Chem. **60**, 452–462 (2022)
42. G. Kaysan, T. Rudszuck, L. Trapp, R. Balbierer, M. Kind, G. Guthausen, Recent applications of NMR diffusion experiments, in *Annual Reports on NMR Spectroscopy* (Academic Press, 2022)

43. E. Flöter, T. Wettlaufer, V. Conty, M. Scharfe, Oleogels—their applicability and methods of characterization. Molecules **26**, 1673 (2021)
44. M.A.D. Guillén, A. Ruiz, High resolution 1H nuclear magnetic resonance in the study of edible oils and fats. Trends Food Sci. Technol. **12**, 328–338 (2001)
45. M.D. Guillén, A. Ruiz, Edible oils: Discrimination by 1H nuclear magnetic resonance. J. Sci. Food Agric. **83**, 338–346 (2003)
46. G. Knothe, J.A. Kenar, Determination of the fatty acid profile by 1H-NMR spectroscopy. Eur. J. Lipid Sci. Technol. **106**, 88–96 (2004)
47. B. Nieva-Echevarría, E. Goicoechea, M.J. Manzanos, M.D. Guillén, A method based on 1H NMR spectral data useful to evaluate the hydrolysis level in complex lipid mixtures. Food Res. Int. **66**, 379–387 (2014)
48. V. Nelis, L. De Neve, S. Danthine, K. Dewettinck, J.C. Martins, P. Van der Meeren, Oil diffusion in fat crystal matrices: characterization by NMR relaxometry and diffusometry. Eur. J. Lipid Sci. Technol. **123**, 2000237 (2021)
49. D.E. Woessner, NMR spin-echo self diffusion measurements on fluids undergoing restricted diffusion. J. Phys. Chem. **67**, 1365–1367 (1963)
50. M. Öğütcü, E. Yilmaz, Characterization of Hazelnut oil oleogels prepared with sunflower and carnauba waxes. Int. J. Food Prop. **18**, 1741–1755 (2015)
51. K.J. Packer, C. Rees, Pulsed NMR studies of restricted diffusion. 1. Droplet size distributions in emulsions. J. Colloid Interface Sci. **40**, 206–218 (1972)
52. R. Bernewitz, G. Guthausen, H.P. Schuchmann, NMR on emulsions: characterisation of liquid dispersed systems. Magn. Reson. Chem. **49**, S93–S104 (2011)
53. M. Adam-Berret, M. Boulard, A. Riaublanc, F. Mariette, Evolution of fat crystal network microstructure followed by NMR. J. Agric. Food. Chem. **59**, 1767–1773 (2011)
54. D. Reische, D. Lillard, R. Eitenmiller, C. Akoh, D. Min, *Food Lipids: Chemistry, Nutrition, and Biotechnology* (CRC Press, New York, 2008)
55. K. Sato, Crystallization behaviour of fats and lipids—a review. Chem. Eng. Sci. **56**, 2255–2265 (2001)
56. C. Liu, Z. Zheng, Z. Meng, X. Chai, C. Cao, Y. Liu, Beeswax and carnauba wax modulate the crystallization behavior of palm kernel stearin. Lwt **115**, 108446 (2019)
57. G.V. Buitimea-Cantúa, S.O. Serna-Saldívar, E. Pérez-Carrillo, T.J. Silva, D. Barrera-Arellano, N.E. Buitimea-Cantúa, Effect of quality of carnauba wax (*Copernica cerífera*) on microstructure, textural, and rheological properties of soybean oil-based organogels. LWT **136**, 110267 (2021)
58. S. Jana, S. Martini, Physical characterization of crystalline networks formed by binary blends of waxes in soybean oil. Food Res. Int. **89**, 245–253 (2016)
59. A. Myerson, *Handbook of Industrial Crystallization* (Butterworth-Heinemann, 2002)
60. R.D. O'brien, *Fats and Oils: Formulating and Processing for Applications* (CRC Press, 2008)
61. F.D. Gunstone, J.L. Harwood, *The Lipid Handbook with CD-ROM* (CRC Press, 2007)
62. S. Ali, A. Tiwari, T. Yeoh, P. Doshi, N. Kelkar, J.C. Shah, J.R. Seth, Crystallization and rheology of mono-and diglycerides and their role in stabilization of emulsion droplets in model topical ointments. Langmuir **38**, 8502–8512 (2022)
63. N. Hedin, T.Y. Yu, I. Furó, Growth of C12E8 micelles with increasing temperature. A convection-compensated PGSE NMR study. Langmuir **16**, 7548–7550 (2000)